Theoretical description of the geometric and electronic structures of organic–organic interfaces in organic solar cells: A brief review

ARTICLE *in* SCIENCE CHINA-CHEMISTRY · OCTOBER 2014

Impact Factor: 1.7 · DOI: 10.1007/s11426-014-5184-x

SCIENCE CHINA
Chemistry

• FEATURE ARTICLES • October 2014 Vol.57 No.10: 1330–1339
• SPECIAL ISSUE • Quantum Chemistry for Extended Systems—In honor of Prof. J.M. André for his 70th birthday doi: 10.1007/s11426-014-5184-x

Theoretical description of the geometric and electronic structures of organic-organic interfaces in organic solar cells: a brief review

FU Yao-Tsung[1], YI YuanPing[1#], COROPCEANU Veaceslav[1], RISKO Chad[1], AZIZ Saadullah G.[2] & BRÉDAS Jean-Luc[1,2*]

[1]*School of Chemistry & Biochemistry and Center for Organic Photonics and Electronics, Georgia Institute of Technology, Atlanta 30332-0400, Georgia, USA*
[2]*Department of Chemistry, King Abdulaziz University, Jeddah 21589, Kingdom of Saudi Arabia*

Received April 9, 2014; accepted May 5, 2014; published online August 29, 2014

We review some of the computational methodologies used in our research group to develop a better understanding of the geometric and electronic structures of organic-organic interfaces present in the active layer of organic solar cells. We focus in particular on the exciton-dissociation and charge-transfer processes at the pentacene-fullerene interface. We also discuss the local morphology at this interface on the basis of molecular dynamics simulations.

organic photovoltaics, organic-organic interface, multi-scale simulations

1 Introduction

The active layer within an organic photovoltaic (OPV) cell [1–12] is composed of a minimum of two distinct materials, an electron-donating/hole-transport material **D** and an electron-accepting/electron-transport material **A**; these have, respectively, a small ionization potential and a large electron affinity. Within this active layer, a combination of optical/electronic processes needs to be optimized for efficient OPV operation:

(1) The initial step involves photoexcitation and formation of bound electron-hole pairs, i.e., excitons. It is important to keep in mind that exciton binding energies in π-conjugated systems usually reach several hundreds of meV. Such high values for the binding energies come from a combination of low dielectric constant, strong electron-electron interactions, and large electron-vibration couplings with the latter leading to substantial geometry relaxations upon excitation or ionization [13]. This is in contrast to the situation in inorganic semiconductors where the exciton binding energy generally reaches only a few meV and, as a result, the electron and the hole can freely separate at room temperature.

(2) Then, prior to decay back to the ground state, the excitons must be able to reach the **D/A** interface; this migration is not influenced by the presence of an electric field as the exciton is charge neutral. Note that, in a number of instances, a strong intermixing of the **D** and **A** species can occur within the active layer, for example, as a result of intercalation of fullerene molecules in between the side-chains of the polymers. In such situations, steps (1) and (2) do effectively merge and the excitons can readily dissociate within less than 100 fs [14, 15].

(3) For exciton dissociation to lead to efficient separation of charge carriers into the **D** component (holes) and **A**

*Corresponding author (email: jean-luc.bredas@chemistry.gatech.edu)
Present address: Key Laboratory of Organic Solids, Beijing National Laboratory for Molecular Sciences (BNLMS), Institute of Chemistry, Chinese Academy of Sciences, Beijing 100190, China

component (electrons), a process that is more complex than a simple electron transfer between **D** and **A** has to follow, since the hole and the electron need to overcome their Coulomb attraction [16].

(4) Once they have separated, the hole and the electron have to migrate towards the electrodes within their respective **D** and **A** phases and avoid bimolecular recombination.

(5) Eventually, the carriers need to be collected efficiently at the electrodes.

Even though the combination of all the steps above has to be optimized, which generally requires a fine balancing act, it can be seen that a most critical process is the dissociation of excitons into electrons and holes at the **D/A** interface and the prevention of (geminate and bimolecular) charge recombination. This will be the focus of Section 2 where we take the example of the pentacene-fullerene interface. In Section 3, we summarize our recent work aimed at characterizing the geometric structure of this pentacene-fullerene **D/A** interface, i.e., the molecular packing between the donor and acceptor molecules (interfacial "morphology").

2 Exciton-dissociation and charge-recombination processes at donor/acceptor interfaces

The optimization of organic solar cells requires a fine balancing act since it involves finding the optimal compromise among a combination of material characteristics that sometimes happen to work in opposite directions. The local **D/A** interface geometry has an impact on the rates of exciton dissociation (which needs to be maximized) and of charge recombination (which decreases the photocurrent and needs to be minimized), as well as on the magnitude of the reverse saturation current in the dark (which needs to be minimized to increase the open-circuit voltage) [17, 18]. Therefore, in order to understand and eventually to develop new strategies to increase the efficiency of organic solar cells, it is crucial to obtain a much better, fundamental understanding of the charge-separation (CS) and charge-recombination (CR) pathways.

The electron-transfer rate of any CS or CR process depends on several factors such as electron-vibration coupling, electronic coupling between reactants and products, and relative free energies of reactants and products. However, to obtain reliable estimates of these parameters on the basis of quantum-chemical approaches represents in general a very difficult task. In particular, a very challenging proposition is the determination of the electronic coupling, since its value is determined by the overlap between the relevant donor and acceptor wave functions. Here, we review the computational approach developed recently in our group [19, 20] that allows the calculation of the electronic coupling between any two molecular (exciton) and charge-transfer states. In contrast to other approaches reported in the literature, this method can be used to evaluate the electronic couplings between electronic states of any spin multiplicity. As a result, the electron-transfer rates involving singlet and triplet states can be computed. We illustrate the application of this methodology to investigate the role that the interface geometry exerts on the efficiency of both exciton-dissociation and charge-recombination processes at model **D/A** interfaces consisting of pentacene/C_{60} complexes [20].

2.1 Evaluation of the electronic couplings and electron-transfer rates

The electronic coupling between the molecular (exciton) and charge-transfer states is a major parameter that controls the dynamics of the charge-separation and charge-recombination processes at **D/A** interfaces. The electronic coupling V_{IF} can be evaluated by a diabatic-state approach (involving the wave functions of the isolated components) that was recently developed in our group [19, 20]:

$$V_{\mathrm{IF}} = \left\langle \Psi^{\mathrm{I}} | H | \Psi^{\mathrm{F}} \right\rangle \tag{1}$$

Here, the initial and final states (Ψ^{I} and Ψ^{F}) are the local (molecular) excited state and charge-transfer state (Ψ^{LE} and Ψ^{CT}) for the exciton-dissociation process or the CT state and ground state for the charge-recombination process, respectively. The states Ψ^{LE} and Ψ^{CT} are spin-adapted diabatic states that are constructed as antisymmetrized products of the isolated donor and acceptor wavefunctions [21]:

$$\Psi_{ij}^{\mathrm{LE}}(\mathrm{S},\mathrm{M}) = \sum\nolimits_{\mathrm{M}_i,\mathrm{M}_j} C_{\mathrm{S}_i\mathrm{M}_i\mathrm{S}_j\mathrm{M}_j}^{\mathrm{SM}} \left| \psi_i^{\mathbf{D}}(\mathrm{S}_i,\mathrm{M}_i)\psi_j^{\mathbf{A}}(\mathrm{S}_j,\mathrm{M}_j) \right| \tag{2}$$

$$\Psi_{kl}^{\mathrm{CT}}(\mathrm{S},\mathrm{M}) = \sum\nolimits_{\mathrm{M}_k,\mathrm{M}_l} C_{\mathrm{S}_k\mathrm{M}_k\mathrm{S}_l\mathrm{M}_l}^{\mathrm{SM}} \left| \psi_k^{\mathbf{D}^+}(\mathrm{S}_k,\mathrm{M}_k)\psi_l^{\mathbf{A}^-}(\mathrm{S}_l,\mathrm{M}_l) \right| \tag{3}$$

where S and M denote the total spin and spin projection of the diabatic states for the donor-acceptor complex; $\psi_m^{\mathbf{D/A}}$ is the m-th excited state of the isolated neutral donor or acceptor with spin S_m and spin projection M_m; and $\psi_m^{\mathbf{D}^+/\mathbf{A}^-}$ corresponds to the oxidized donor or reduced acceptor. The $C_{\mathrm{S}_k\mathrm{M}_k\mathrm{S}_l\mathrm{M}_l}^{\mathrm{SM}}$ terms represent the Clebsch-Gordan coefficients that result in the linear combination of the isolated wavefunction products to be an eigenfunction of the total spin. For the sake of simplicity, we can compute the isolated excited and charged states and then the electronic couplings in the framework of the semiempirical intermediate neglect of differential overlap (INDO) Hamiltonian [22] coupled to a single configuration interaction (SCI) scheme.

When the CT states and/or the local-excited states are orbitally degenerate (as in the case of C_{60} and its derivatives), an effective electronic coupling (V_{eff}) can be calculated by the following equation:

$$V_{\mathrm{eff}}^2 = \frac{1}{\mathrm{g}_I} \sum\nolimits_{i,j,k,l} \left\langle \Psi_{ij}^{I} | H | \Psi_{kl}^{F} \right\rangle^2 \tag{4}$$

where g_I is the orbital multiplicity of the initial diabatic state,

and can be calculated as the product of the multiplicities of the initial monomer states ($g_i \times g_j$).

According to the semi-classical model of Marcus electron-transfer theory, the rates of exciton dissociation and charge recombination can be estimated as [23, 24]:

$$k_{\mathrm{IF}} = V_{\mathrm{IF}}^2 \sqrt{\frac{\pi}{\lambda k_{\mathrm{B}} T \hbar^2}} \exp\left[-\frac{\left(\Delta G^0 + \lambda\right)^2}{4\lambda k_{\mathrm{B}} T}\right] \quad (5)$$

where k_{B} and $\hbar$ denote the Boltzmann and Planck constants, respectively; T is the temperature (set to 300 K in our calculations); λ represents the reorganization energy and ΔG^0 is the Gibbs free energy of the electron-transfer reaction.

If we ignore the entropy contribution, ΔG^0 can be estimated as the energy difference between the diabatic initial and final states. The energy of the diabatic states is composed of the total energies of the isolated states of the donor and acceptor and the Coulomb energy between the donor and acceptor. The Coulomb energy can be computed as the sum of the Coulombic interactions between the atomic charges of the donor and acceptor; for instance, the Coulomb energy between the donor cation and acceptor anion can be written as:

$$E_{\mathrm{coul}}^{\mathbf{D}^+/\mathbf{A}^-} = \sum\nolimits_{\mathbf{d}\in\mathbf{D}^+,\mathbf{a}\in\mathbf{A}^-} \frac{q_{\mathbf{d}} q_{\mathbf{a}}}{4\pi\varepsilon_0 \varepsilon r_{\mathbf{da}}} \quad (6)$$

where $q_{\mathbf{d}}$ and $q_{\mathbf{a}}$ are the partial charges (which can be obtained via an INDO Mulliken population analysis) on atom **d** of the donor cation and atom **a** of the acceptor anion, respectively; $r_{\mathbf{da}}$ is the distance between atoms **d** and **a**; ε_0 is the vacuum permittivity and ε corresponds to the medium. The results show that the Coulomb energies for the diabatic local (i.e., intramolecular) states of the **D/A** complexes are vanishingly small, while those for the diabatic CT states become very significant. Thus, using the total energy of the diabatic ground state as the reference, the energies of the local-excited states for the **D/A** complexes are approximated as the excitation energies of the isolated molecules; on the other hand, the energy of the lowest CT state must include the contribution from the Coulomb interactions:

$$E_{\mathrm{CT}} = IP^{\mathbf{D}} + EA^{\mathbf{A}} + E_{\mathrm{coul}}^{\mathbf{D}^+/\mathbf{A}^-} \quad (7)$$

where $IP^{\mathbf{D}}$ is the ionization potential of the donor and $EA^{\mathbf{A}}$ is the electron affinity of the acceptor.

2.2 The pentacene-C_{60} complex

Using this methodology, we have investigated the role of the pentacene/C_{60} interface geometry on the efficiency of both exciton-dissociation and charge-recombination processes, namely to rationalize some of the differences in performance between the bilayer and bulk-heterojunction architectures [20]. Figure 1(a) illustrates the model complex configurations we have considered (a more detailed discussion of the energetics of these configurations can be found in Section 3). We have calculated the electronic couplings and rates for exciton dissociation and charge recombination as a function of intermolecular distance and the rotation angle or lateral displacement of pentacene.

The calculated electronic couplings involving the lowest CT state (CT_0) for the perpendicular and parallel configurations of the pentacene/C_{60} complex as a function of the intermolecular distance are shown in Figure 1(b). For the same intermolecular distance, the electronic couplings obtained in the case of parallel configurations are significantly larger

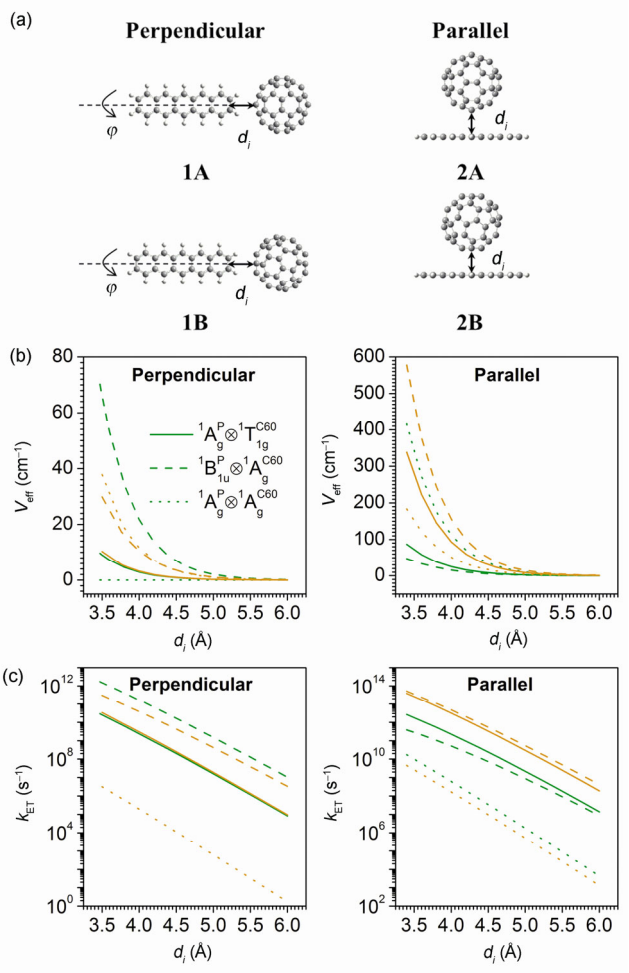

Figure 1 Illustration of the pentacene/C_{60} configurations (a) and dependence of the electronic couplings (b) and rates (c) for exciton dissociation (from molecular excited states $^1A_g^P \otimes {}^1T_{1g}^{C60}$ (solid lines) and $^1B_{1u}^P \otimes {}^1A_g^{C60}$ (dashed lines) to the lowest CT state, $^2B_{2g}^{P+} \otimes {}^2T_{1u}^{C60-}$) and charge recombination (from the lowest CT state to the ground state: $^2B_{2g}^{P+} \otimes {}^2T_{1u}^{C60-} \rightarrow {}^1A_g^P \otimes {}^1A_g^{C60}$ (dotted lines)), as a function of intermolecular distance, d_i; green lines refer to orientations 1A and 2A and orange lines to orientations 1B and 2B. In the calculations of rates, we make use of the experimental values for energies estimated from the condensed phase: the S_1 energy is 1.7 eV for C_{60} [25] and 1.85 eV for pentacene [26, 27], IP(P) = 5.1 eV [28] and EA(C_{60}) = –3.5 eV [29]; the reorganization energy is set to 0.5 eV. In the case of orientation 1A, the CR rate is equal to zero due to the vanishing coupling. Adapted from Ref. [20].

than in the case of perpendicular orientations; for the intermolecular distance corresponding to the sum of the van der Waals radii of the closest atoms of pentacene and C_{60} molecules (which represents the smallest intermolecular distance considered here), the electronic coupling can be as large as 75 meV. Except for the case of orientation 1A (pentacene perpendicular to a C=C edge, Figure 1(a)) where due to symmetry reasons there is no interaction between the ground state and the CT_0 state, the respective coupling is significant in all other cases. The electronic couplings for all states show the expected exponential dependence on intermolecular distance.

The lowest excited CT states (CT_1, CT_2) arise from the first excited state of the radical anion of C_{60} and the cation of pentacene; from electronic absorption spectra, these two states are located 1.15 [30, 31] and 1.31 eV [32], respectively, above the corresponding ground states of the charged species. The electronic couplings between the lowest molecular excited states and the lowest excited CT states (CT_1 and CT_2) show trends very similar to those derived for CT_0, (Figure 2). However, since in this simple complex the CT_1 and CT_2 states are much higher in energy than the CT_0 state, the latter is expected to play the most significant role in the exciton dissociation process, as detailed below.

As shown in Figure 1(c), the calculated CT and CR rates underline that, for typical intermolecular distances of ~3.5–4.5 Å between adjacent molecules, the electron-transfer rates from local (intramolecular) excited states to the lowest

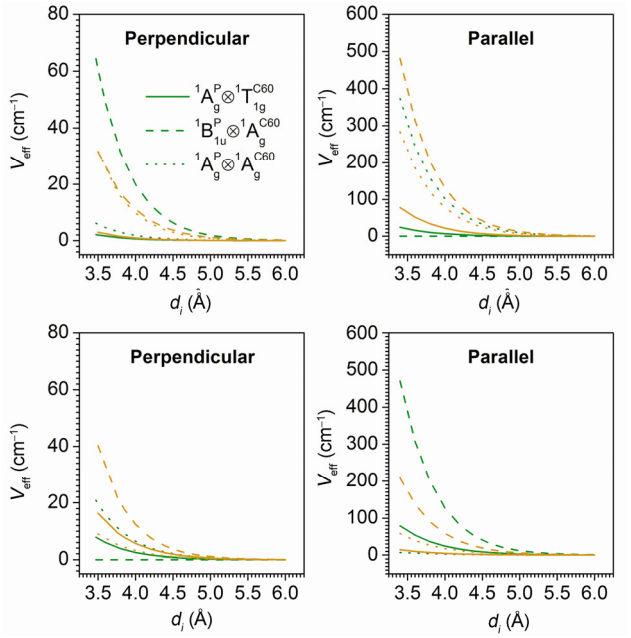

Figure 2 Electronic couplings of the ground state ($^1A_g^P \otimes {}^1A_g^{C60}$ (dotted lines)) and local-excited singlet states ($^1A_g^P \otimes {}^1T_{1g}^{C60}$ (solid lines) and $^1B_{1u}^P \otimes {}^1A_g^{C60}$ (dashed lines)) with the CT_1 (upper panels) and CT_2 (lower panels) states, as a function of intermolecular distance for the perpendicular orientations 1A and 1B and parallel orientations 2A and 2B illustrated in Figure 1; green lines refer to orientations 1A and 2A and orange lines to orientations 1B and 2B. Adapted from Ref. [20].

CT state can be very large. These rates can reach ~10^{10}–10^{12} s^{-1} even in the case of perpendicular configurations of the complex that do not lead to large electronic couplings; the results indicate that for such orientations pentacene-based excitons dissociate at least ten times faster than fullerene-based excitons. When going from perpendicular to parallel configurations, there occurs a significant increase in the dissociation rate for fullerene-based excitons that comes from an increase in the related electronic coupling and driving force. In the case of electron transfer from the lowest excited state of pentacene, the CT rate significantly increases for the "hexagon"-type parallel geometry 2B (where a fullerene hexagon directly faces pentacene); for the "edge"-type configuration 2A (where a fullerene C–C bond directly faces pentacene), the rate is similar to that in the perpendicular orientation 1A. Thus, our calculations suggest that, irrespective of the geometrical configurations of the interface, both types of excitons, whether formed on the pentacene molecule or on the C_{60} molecule, are able to dissociate efficiently.

It is also important to discuss the charge-recombination rates between the lowest CT state and the ground state. As seen from Figure 1, the CR rates can be very large for parallel configurations of the complex, reaching values over 10^{10} s^{-1}. In the case of "hexagon"-type perpendicular configurations, the CR rates are below 10^7 s^{-1} even for small intermolecular distances. Moreover, in the case of "edge"-type configurations, as a result of the weak electronic interactions, the CR rates become vanishingly small. Very small CR rates are also found for parallel but significantly displaced configurations of the complex.

Thus, our results suggest that in the case of pentacene/fullerene bilayer architectures, where the **D/A** molecular pairs are expected to be found mainly in perpendicular or displaced-parallel orientations, the CR processes from the CT state should play less of a significant role than in the case of bulk heterojunctions, where a substantial number of pentacene/fullerene complexes should be found in parallel configurations. In the latter case, the CR process could therefore compete efficiently with the dissociation of the CT states into mobile charge carriers and constitute an adverse factor limiting device performance.

A clear evidence of the dependence of power conversion efficiency on the heterojunction morphology was recently described in bilayer zinc phthalocyanine (ZnPc)/C_{60} solar cells [33]. Devices based on bilayers where C_{60} is deposited on top of a ZnPc layer at the surface of which the ZnPc molecules lie flat (parallel or face-on configurations) show a larger power conversion efficiency than those where the ZnPc molecules stand up (perpendicular configurations). Based on the experimental data and on calculations of the electronic couplings similar to those detailed above for pentacene/C_{60}, it was found that the main contributor to this difference is the more efficient exciton dissociation for face-on configurations.

It is important to bear in mind that while the consideration of model complexes made of a single donor and a single acceptor can provide some useful insight for the understanding of the interfacial electronic processes, it is far from being sufficient. Indeed, electronic interactions among adjacent donor molecules and among adjacent acceptor molecules can result in the formation of CT states that are effectively delocalized over several molecules [15]. It is clear that the development of suitable models for the description of such delocalized states and of the related dynamical processes would represent a major step towards a detailed understanding of charge separation at **D/A** interfaces in organic solar cells. This is also the reason why it is critical to obtain a reliable description of the interfacial packing configurations ("local" morphology) between and among **D** and **A** molecules, which is the focus of Section 3.

3 Molecular dynamics description of the pentacene-C_{60} interface

We now turn our attention to the nature of the morphology at the **D/A** interfaces. Recent experimental evidence has shone new light on the morphological complexity of these interfaces [34–49]. The relative miscibility of the **D** and **A** components, the deposition protocol (e.g., vacuum deposition, solution casting, or spin coating to name but a few [50–52]), and a variety of post-processing procedures (e.g., solvent and thermal annealing or solvent additives) impact not only the properties of the "bulk" materials but can lead to potentially dramatic changes to the interface morphology [53]. Here, as a first step, we consider a relatively "simple" bilayer interface with pentacene as the electron donor and C_{60} as the electron acceptor [17, 54–61].

The relatively small size and rigid structural characteristics of these molecules has also allowed the pentacene-C_{60} interface to be considered in a number of theoretical investigations, ranging from electronic-structure calculations on molecular complexes, as described in Section 2, to atomistic molecular dynamics (MD) simulations [20, 62–69]. Using MD simulations (employing the MM3 force field of Allinger and co-workers [70]), we have probed on a larger scale the nature of the pentacene-C_{60} interface, with a particular emphasis on an architecture in which the C_{60} layer resides on top of the pentacene layer (the common motif used in conventional pentacene-C_{60} bilayer devices) [71]. We were particularly interested in delineating how the nature of the pentacene surface—either the (001) surface where the molecules stand upright (nearly perpendicular) to the surface, or the (010) surface for which the molecules lie parallel to the surface—influences the characteristics of the interface with C_{60}. We also considered what consequence terraced (or stepped) pentacene surfaces may have; the formation of terraced surfaces is determined by the surface energy, roughness, and temperature of the substrate on which the pentacene film is deposited along with deposition temperature and rates [72–75].

As a preliminary step, it is thus useful to understand the strength of the interactions between pentacene and C_{60} over different scales. Energy-minimization calculations (MM3) were employed to analyze the binding energy of a single pentacene-C_{60} complex as a function of distance and pentacene orientation. The calculations indicate, as could be intuitively expected, that pentacene and C_{60} are more strongly bound when the pentacene face is parallel with the C_{60} cage (−9.44 and −8.92 kcal/mol when the pentacene center of mass is aligned with the five- and six-membered ring on the C_{60}, respectively) vs. perpendicular (−2.27 and −2.40 kcal/mol for interactions with the five- and six-membered ring on the C_{60}, respectively). Analysis of the cohesive (adsorption) energy of a single C_{60} on the pentacene surfaces of interest is consistent with this picture. The MM3 results show that C_{60} preferentially binds to the pentacene (010) face (33.5 ± 2 kcal/mol) vs. the (001) face (18.9 ± 2 kcal/mol); these trends also agree with previous estimates (that also take into account various polymorphs) [62, 65, 67], even though different pentacene models were used.

In addition, we evaluated the surface energies for pentacene and C_{60}, as stronger interfacial interactions between surfaces can be expected when the surface energies are most similar. The MM3 surface energies show trends similar to these for the complex binding energies and cohesive energy for a single C_{60} on a pentacene surface. For pentacene, the surface energies for the (001) and (010) are 53.0 and 91.8 mJ/m^2, respectively; periodic slab calculations employing density functional theory (DFT) have determined the energies of these faces to be 49.7 and 76.9 mJ/m^2, respectively [76]. On the other hand, contact angle measurements have derived a surface energy of approximately 34–38 mJ/m^2 for the thin-film pentacene structure that is expected to present mainly an (001) surface with the pentacene molecules standing up [72, 77]; the notable differences with respect to the calculations, however, can be due to the difficulty in identifying the exact geometrical parameters of the thin-film pentacene used in the experiment (including the phases, planes, and any surface reconstruction). For C_{60}, the calculated surface energies of the (001) and hexagonal-close packed (h.c.p.) faces are 98.5 and 88.0 mJ/m^2, respectively (again, there is deviation with the empirically-determined C_{60} surface energy of approximately 42 mJ/m^2) [78–84]. As a first approximation based on the results from all these evaluations, it should be anticipated that C_{60} will interact more strongly with the pentacene (010) surface than the (001) surface, given their more similar surface energies.

To describe the morphology of the pentacene-C_{60} interface, we considered MD simulations with up to 105 fullerenes randomly distributed on the "pristine" pentacene (001) and pentacene (010) surfaces (Figure 3). For pentacene (001), the presence of C_{60} leads to a structural change of the top layer. The fullerenes position themselves in the divots

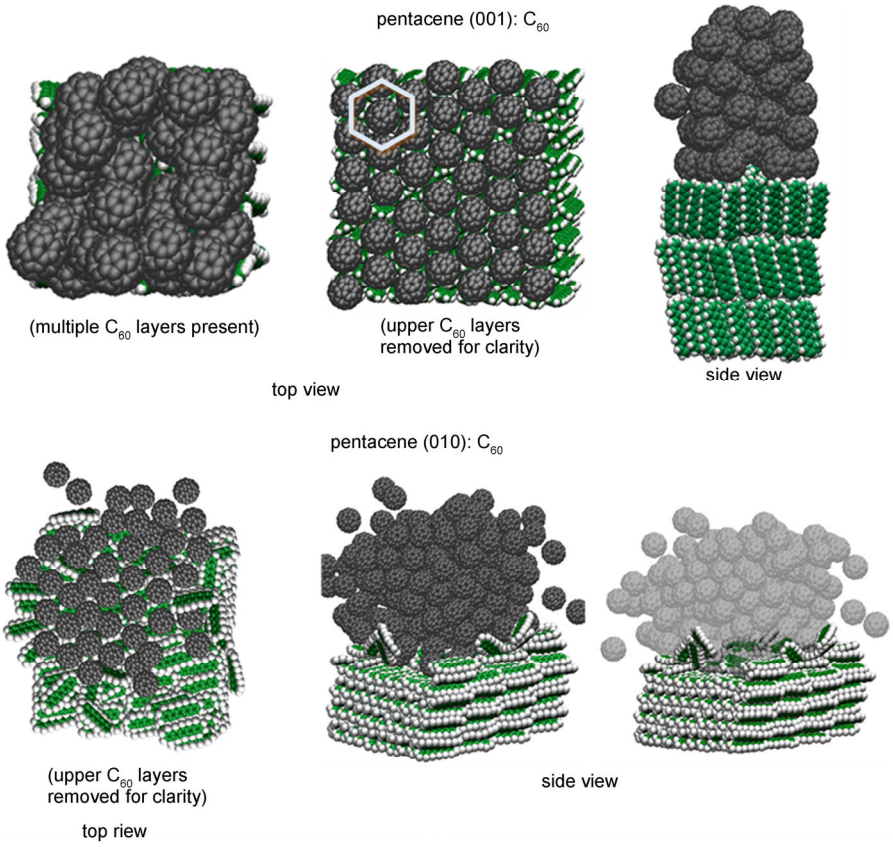

Figure 3 Snapshots of the top and side views after 600 ps simulations for the (top) pentacene (001):C_{60} interface and (bottom) pentacene (010):C_{60} interface. Note that some of the fullerenes have been removed or made transparent to aid visualization. Adapted from Ref. [71].

between the pentacene molecules. As the fullerene content increases, the first fullerene layer takes on the hexagonal closed pack configuration reported for fullerenes [67, 81, 84], with the additional layers taking on the same packing configuration.

When C_{60} is deposited on the pentacene (010) surface, however, there is a considerable rearrangement of the upper pentacene layers within a very short period of time due to the increased intermolecular interactions noted above. The fullerenes tend to sit in the middle portion of the pentacene molecules and eventually "burrow" or displace the pentacene molecules in the upper layer(s), consistent with previous results of C_{60} on the pentacene (010) surface [67]. Importantly, this leads to interfacial disorder and intermixing within the top pentacene layer (Figure 3). These results suggest that fullerenes deposited on the (010) surface should lead to a mixed structure right at the interface between the two materials, in stark contrast with what is seen for the pentacene (001) surface.

As mentioned above, the surface energy, roughness, and temperature of the substrate on which the pentacene film is deposited can have a considerable impact on the interface as terraced surfaces could be prevalent. To consider such situations, a series of terraced surfaces were constructed. Again, significant disorder and intermixing of the pentacene and C_{60} molecules is observed (Figure 4). For the predominantly pentacene (001) structures, which previously showed minimal interactions between the pentacene and C_{60} layers, the pentacene molecules along the now open (0–10) and (100) faces readily disorder and intermix with the C_{60} molecules. There is also disruption of the molecular packing of the pentacene layers underneath the exposure. For terraces created in pristine pentacene (010) surfaces, the degree of disorder and interdiffusion is even larger, as one might expect from the results on the pristine surfaces.

The results of these simulations, in agreement with a growing number of experimental [33, 47, 48, 85] and theoretical [49, 53, 86] results for polymer-fullerene blends and molecule-molecule and polymer-molecule bilayer architectures, reveal large degrees of disorder among the pentacene and C_{60} molecules depending on the crystalline face on which the fullerenes are deposited and the presence of terraces. In particular, the details of the simulations are consistent with the results of time-of-flight secondary ion mass spectroscopy (TOF-SIMS) experiments on copper phthalocyanine (CuPc)-C_{60} interfaces that reveal an intermixed layer of 6.5 nm when C_{60} is deposited on CuPc (and 2.7 nm when the deposition order is reversed) [46], as well as a MD simulation study on pentacene interfaces with perylene-

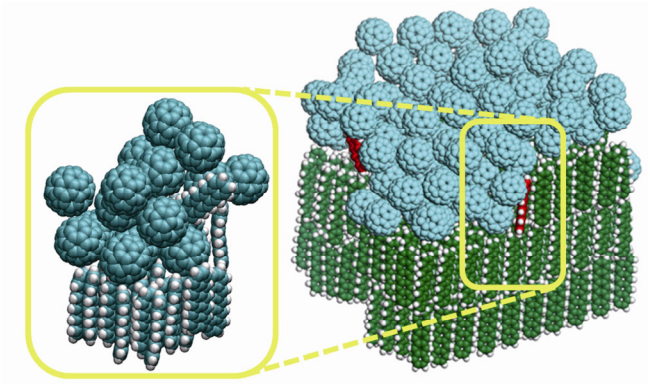

Figure 4 Representative example of the disorder and intermixing of pentacene and C_{60} on a terraced pentacene (001) surface.

3,4,9,10-tetracarboxylic-3,4,9,10-dianhydride (PTCDA) [49].

The growing evidence of these complex "local" interface morphologies, as indicated above, lead to ambiguity pertaining to the underlying physical mechanisms behind OPV operation and how one might design new molecular structures to develop appropriate active-layer architectures. It is currently not clear what role disorder and intermixing play, as such effects seemingly show different behavior as a function of the active-layer construct. Groves and co-workers [53] have elegantly shown that for BHJ architectures that smooth (sharp) interfaces should lead to more efficient OPVs vs. those with rough (intermixed) interfaces. On the other hand, a number of researchers are intrigued by the electronic and optical properties of the amorphous, highly intermixed regions in BHJ cells and their ultimate function. Regarding their superb performance in BHJ cells, a recently hypothesized key attribute of fullerene derivatives is precisely their general ability to, at the same time, form well-ordered domains and intermix with polymers [43]. Also, in the case of bilayer architectures, Zimmerman *et al.* [85] have shown that controlled disorder at the interface can minimize charge recombination, while improved bulk crystallinity increases both exciton- and charge-transport efficiency.

4 Conclusions

Our discussion has underlined that, when developing design rules regarding the synthesis of new molecular and polymeric materials for OPV, it is not enough to consider the intrinsic energetics of the charged and excited states of the individual components. Ultimately, there is a critical need to consider as well: (1) the active-layer architecture in which the material will be employed; (2) the material miscibility not only in solution (if the active layer is to be solution processed) but also with the other active component; (3) the post-processing procedure, since each of these can present a tremendous impact on the OPV power conversion efficiency. To comprehend all these aspects will require multiscale simulations—some of which have been outlined here—and controlled experiments to fully understand and appreciate the complexity of the bulk and interfacial structures/morphologies and how these impact the intrinsic molecular (or polymer) characteristics. It is only when armed with such a detailed knowledge, that one could begin to rationalize design principles leading to more efficient OPV materials.

For multiscale simulations to reach an integrated description of the exciton-dissociation, charge-separation, and (geminate and bimolecular) charge-recombination processes, multiple challenges must be met [10]. These include:

(1) The development of quantum-mechanical methodologies able to describe reliably the CT and CS states on a large (meso) scale involving many **D** and **A** chain segments/molecules. While popular DFT methodologies tend to over delocalize the wave functions, and therefore underestimate the CT energies, Hartree-Fock-based methods suffer from too much localization. Modern long-range-corrected DFT functionals could provide a way forward [87–92].

(2) The development of hybrid quantum mechanics/molecular mechanics (QM/MM) methodologies where the MM part needs to provide an adequate description of the polarization phenomena occurring upon charge separation, which requires appropriate polarizable force fields [93, 94].

(3) The development of molecular dynamics (MD) methodologies that, given the absence of experimental data with the necessary nanoscale (molecular) resolution, can provide adequate, reliable descriptions of the local morphologies at **D/A** interfaces. This is an important part of the problem indeed as the work we described in Section 2 has demonstrated that the rates of exciton dissociation dramatically depend on the way **D** and **A** chain segments/molecules pack at their interfaces.

(4) The development of Monte Carlo methodologies to describe the rates of the charge-transport and bimolecular charge-recombination processes as a function of the energetic landscape within the active layer [95].

This work was supported by the Deanship of Scientific Research of King Abdulaziz University under an International Collaboration Grant (D-001-433), the Office of Naval Research (N00014-14-1-0171 P00001), and the National Science Foundation under the STC Program (DMR-0120967) and the CRIF Program (CHE-0946869).

1 Morel DL, Ghosh AK, Feng T, Stogryn EL, Purwin PE, Shaw RF, Fishman C. High-efficiency organic solar cells. *Appl Phys Lett*, 1978, 32: 495–497
2 Tang CW. Two-layer organic photovoltaic cell. *Appl Phys Lett*, 1986, 48: 183–185
3 Hiramoto M, Fujiwara H, Yokoyama M. Three-layered organic solar cell with a photoactive interlayer of codeposited pigments. *Appl Phys Lett*, 1991, 58: 1062–1064
4 Halls JJM, Walsh CA, Greenham NC, Marseglia EA, Friend RH, Moratti SC, Holmes AB. Efficient photodiodes from interpenetrating

polymer networks. *Nature*, 1995, 376: 498–500
5 Yu G, Gao J, Hummelen JC, Wudl F, Heeger AJ. Polymer photovoltaic cells: enhanced efficiencies via a network of internal donor-acceptor heterojunctions. *Science*, 1995, 270: 1789–1791
6 Risko C, McGehee MD, Bredas JL. A quantum-chemical perspective into low optical-gap polymers for highly-efficient organic solar cells. *Chem Sci*, 2011, 2: 1200–1218
7 Potscavage WJ, Sharma A, Kippelen B. Critical interfaces in organic solar cells and their influence on the open-circuit voltage. *Acc Chem Res*, 2009, 42: 1758–1767
8 Anthony JE, Facchetti A, Heeney M, Marder SR, Zhan X. N-type organic semiconductors in organic electronics. *Adv Mater*, 2010, 22: 3876–3892
9 Kippelen B, Bredas JL. Organic photovoltaics. *Energy Environ Sci*, 2009, 2: 251–261
10 Bredas JL, Norton JE, Cornil J, Coropceanu V. Molecular understanding of organic solar cells: the challenges. *Acc Chem Res*, 2009, 42: 1691–1699
11 Hoppe H, Sariciftci NS. Organic solar cells: an overview. *J Mater Res*, 2004, 19: 1924–1945
12 Thompson BC, Fréchet JMJ. Polymer-fullerene composite solar cells. *Angew Chem Int Ed*, 2008, 47: 58–77
13 Bredas JL, Street GB. Polarons, bipolarons, and solitons in conducting polymers. *Acc Chem Res*, 1985, 18: 309–315
14 Banerji N, Cowan S, Leclerc M, Vauthey E, Heeger AJ. Exciton formation, relaxation, and decay in PCDTBT. *J Am Chem Soc*, 2010, 132: 17459–17470
15 Gélinas S, Rao A, Kumar A, Smith SL, Chin AW, Clark J, van der Poll TS, Bazan GC, Friend RH. Ultrafast long-range charge separation in organic semiconductor photovoltaic diodes. *Science*, 2014, 343: 512–516
16 Bredas JL. When electrons leave holes in organic solar cells. *Science*, 2014, 343: 492–493
17 Potscavage WJ, Yoo S, Kippelen B. Origin of the open-circuit voltage in multilayer heterojunction organic solar cells. *Appl Phys Lett*, 2008, 93: 193308
18 Perez MD, Borek C, Forrest SR, Thompson ME. Molecular and morphological influences on the open circuit voltages of organic photovoltaic devices. *J Am Chem Soc*, 2009, 131: 9281–9286
19 Kawatsu T, Coropceanu V, Ye A, Bredas JL. Quantum-chemical approach to electronic coupling: application to charge separation and charge recombination pathways in a model molecular donor-acceptor system for organic solar cells. *J Phys Chem C*, 2008, 112: 3429–3433
20 Yi Y, Coropceanu V, Bredas JL. Exciton-dissociation and charge-recombination processes in pentacene/C60 solar cells: theoretical insight into the impact of interface geometry. *J Am Chem Soc*, 2009, 131: 15777–15783
21 Edmonds AR. *Angular Momentum in Quantum Mechanics*. Princeton: Princeton University Press, 1985
22 Ridley J, Zerner M. Intermediate neglect of differential overlap technique for spectroscopy: pyrrole and azines. *Theor Chim Acta*, 1973, 32: 111–134
23 Marcus RA. Electron transfer reactions in chemistry. Theory and experiment. *Rev Mod Phys*, 1993, 65: 599–610
24 Barbara PF, Meyer TJ, Ratner MA. Contemporary issues in electron transfer research. *J Phys Chem*, 1996, 100: 13148–13168
25 Akimoto I, Ashida M, Kan'no K. Luminescence from C60 single crystals in glassy phase under site-selective excitation. *Chem Phys Lett*, 1998, 292: 561–566
26 Jundt C, Klein G, Sipp B, Lemoigne J, Joucla M, Villaeys AA. Exciton dynamics in pentacene thin-films studied by pump-probe spectroscopy. *Chem Phys Lett*, 1995, 241: 84–88
27 Faltermeier D, Gompf B, Dressel M, Tripathi AK, Pflaum J. Optical properties of pentacene thin films and single crystals. *Phys Rev B*, 2006, 74: 125416
28 Hwang J, Wan A, Kahn A. Energetics of metal-organic interfaces: new experiments and assessment of the field. *Mat Sci Eng R*, 2009, 64: 1–31
29 Schwedhelm R, Kipp L, Dallmeyer A, Skibowski M. Experimental band gap and core-hole electron interaction in epitaxial C60 films. *Phys Rev B*, 1998, 58: 13176–13180
30 Kato T, Kodama T, Shida T, Nakagawa T, Matsui Y, Suzuki S, Shiromaru H, Yamauchi K, Achiba Y. Electronic absorption spectra of the radical anions and cations of fullerenes: C60 and C70. *Chem Phys Lett*, 1991, 180: 446–450
31 Kato T, Kodama T, Shida T. Spectroscopic studies of the radical anion of C60. Detection of the fluorenscence and reinvestigation of the ESR spectrum. *Chem Phys Lett*, 1993, 205: 405–409
32 Szczepanski J, Wehlburg C, Vala M. Vibrational and electronic-spectra of matrix-isolated pentacene cations and anions. *Chem Phys Lett*, 1995, 232: 221–228
33 Rand BP, Cheyns D, Vasseur K, Giebink NC, Mothy S, Yi YP, Coropceanu V, Beljonne D, Cornil J, Bredas JL, Genoe J. The impact of molecular orientation on the photovoltaic properties of a phthalocyanine/fullerene heterojunction. *Adv Funct Mater*, 2012, 22: 2987–2995
34 Campoy-Quiles M, Ferenczi T, Agostinelli T, Etchegoin PG, Kim Y, Anthopoulos TD, Stavrinou PN, Bradley DDC, Nelson J. Morphology evolution via self-organization and lateral and vertical diffusion in polymer: fullerene solar cell blends. *Nat Mater*, 2008, 7: 158–164
35 Mayer AC, Toney MF, Scully SR, Rivnay J, Brabec CJ, Scharber M, Koppe M, Heeney M, McCulloch I, McGehee MD. Bimolecular crystals of fullerenes in conjugated polymers and the implications of molecular mixing for solar cells. *Adv Funct Mater*, 2009, 19: 1173–1179
36 Collins BA, Gann E, Guignard L, He X, McNeill CR, Ade H. Molecular miscibility of polymer-fullerene blends. *J Phys Chem Lett*, 2010, 1: 3160–3166
37 Chen D, Nakahara A, Wei D, Nordlund D, Russell TP. P3HT/PCBM bulk heterojunction organic photovoltaics: correlating efficiency and morphology. *Nano Lett*, 2010, 11: 561–567
38 Szarko JM, Guo J, Liang Y, Lee B, Rolczynski BS, Strzalka J, Xu T, Loser S, Marks TJ, Yu L, Chen LX. When function follows form: effects of donor copolymer side chains on film morphology and BHJ solar cell performance. *Adv Mater*, 2010, 22: 5468–5472
39 Yin W, Dadmun M. A new model for the morphology of P3HT/PCBM organic photovoltaics from small-angle neutron scattering: rivers and streams. *Acs Nano*, 2011, 5: 4756–4768
40 Lu H, Akgun B, Russell TP. Morphological characterization of a low-bandgap crystalline polymer: PCBM bulk heterojunction solar cells. *Adv Energy Mater*, 2011, 1: 870–878
41 Parnell AJ, Cadby AJ, Mykhaylyk OO, Dunbar ADF, Hopkinson PE, Donald AM, Jones RAL. Nanoscale phase separation of P3HTPCBM thick films as measured by small-angle X-ray scattering. *Macromolecules*, 2011, 44: 6503–6508
42 Collins BA, Tumbleston JR, Ade H. Miscibility, crystallinity, and phase development in P3HT/PCBM solar cells: toward an enlightened understanding of device morphology and stability. *J Phys Chem Lett*, 2011, 2: 3135–3145
43 Jamieson FC, Domingo EB, McCarthy-Ward T, Heeney M, Stingelin N, Durrant JR. Fullerene crystallisation as a key driver of charge separation in polymer/fullerene bulk heterojunction solar cells. *Chem Sci*, 2012, 3: 485–492
44 Miller NC, Sweetnam S, Hoke ET, Gysel R, Miller CE, Bartelt JA, Xie X, Toney MF, McGehee MD. Molecular packing and solar cell performance in blends of polymers with a bisadduct fullerene. *Nano Lett*, 2012, 12: 1566–1570
45 Treat ND, Brady MA, Smith G, Toney MF, Kramer EJ, Hawker CJ, Chabinyc ML. Interdiffusion of PCBM and P3HT reveals miscibility in a photovoltaically active blend. *Adv Energy Mater*, 2011, 1: 82–89
46 Sai N, Gearba R, Dolocan A, Tritsch JR, Chan WL, Chelikowsky JR, Leung K, Zhu X. Understanding the interface dipole of copper phthalocyanine (CuPc)/C60: theory and experiment. *J Phys Chem Lett*, 2012, 3: 2173–2177
47 Loiudice A, Rizzo A, Biasiucci M, Gigli G. Bulk heterojunction versus diffused bilayer: the role of device geometry in solution p-doped polymer-based solar cells. *J Phys Chem Lett*, 2012, 3:

1908–1915
48 Loiudice A, Rizzo A, Latini G, Nobile C, de Giorgi M, Gigli G. Graded vertical phase separation of donor/acceptor species for polymer solar cells. *Sol Energ Mat Sol C*, 2012, 100: 147–152
49 Poschlad A, Meded V, Maul R, Wenzel W. Different interface orientations of pentacene and PTCDA induce different degrees of disorder. *Nanoscale Res Lett*, 2012, 7: 248
50 Brabec CJ, Durrant JR. Solution-processed organic solar cells. *Mrs Bull*, 2008, 33: 670–675
51 Helgesen M, Sondergaard R, Krebs FC. Advanced materials and processes for polymer solar cell devices. *J Mater Chem*, 2010, 20: 36–60
52 Krebs FC. Fabrication and processing of polymer solar cells: a review of printing and coating techniques. *Sol Energ Mat Sol C*, 2009, 93: 394–412
53 Lyons BP, Clarke N, Groves C. The relative importance of domain size, domain purity and domain interfaces to the performance of bulk-heterojunction organic photovoltaics. *Energy Environ Sci*, 2012, 5: 7657–7663
54 Yoo S, Domercq B, Kippelen B. Efficient thin-film organic solar cells based on pentacene/C_{60} heterojunctions. *Appl Phys Lett*, 2004, 85: 5427–5429
55 Pandey AK, Nunzi JM. Efficient flexible and thermally stable pentacene/C60 small molecule based organic solar cells. *Appl Phys Lett*, 2006, 89: 213506
56 Yang YC, Chang CH, Lee YL. Complexation of fullerenes on a pentacene-modified Au(111) surface. *Chem Mater*, 2007, 19: 6126–6130
57 Al-Mahboob A, Sadowski JT, Fujikawa Y, Nakajima K, Sakurai T. Kinetics-driven anisotropic growth of pentacene thin films. *Phys Rev B*, 2008, 77: 035426
58 Dougherty DB, Jin W, Cullen WG, Dutton G, Reutt-Robey JE, Robey SW. Local transport gap in C_{60} nanochains on a pentacene template. *Phys Rev B*, 2008, 77: 073414
59 Conrad BR, Tosado J, Dutton G, Dougherty DB, Jin W, Bonnen T, Schuldenfrei A, Cullen WG, Williams ED, Reutt-Robey JE, Robey SW. C60 cluster formation at interfaces with pentacene thin-film phases. *Appl Phys Lett*, 2009, 95: 213302
60 Dougherty DB, Jin W, Cullen WG, Reutt-Robey JE, Robey SW. Striped domains at the pentacene: C_{60} interface. *Appl Phys Lett*, 2009, 94: 023103
61 Jin W, Dougherty DB, Cullen WG, Robey S, Reutt-Robey JE. C60-pentacene network formation by 2-d co-crystallization. *Langmuir*, 2009, 25: 9857–9862
62 Cantrell R, Clancy P. A computational study of surface diffusion of C60 on pentacene. *Surf Sci*, 2008, 602: 3499–3505
63 Verlaak S, Beljonne D, Cheyns D, Rolin C, Linares M, Castet F, Cornil J, Heremans P. Electronic structure and geminate pair energetics at organic-organic interfaces: the case of pentacene/C60 heterojunctions. *Adv Funct Mater*, 2009, 19: 3809–3814
64 Zheng Y, Pregler SK, Myers JD, Ouyang JM, Sinnott SB, Xue JG. Computational and experimental studies of phase separation in pentacene:C60 mixtures. *J Vac Sci Technol B*, 2009, 27: 169–179
65 Cantrell R, Clancy P. A molecular dynamics study of the effect of pentacene polymorphs on C_{60} surface adsorption and diffusional properties and the tendency to form nanowires. *Mol Simulat*, 2010, 36: 590–603
66 Linares M, Beljonne D, Cornil J, Lancaster K, Bredas JL, Verlaak S, Mityashin A, Heremans P, Fuchs A, Lennartz C, Ide J, Mereau R, Aurel P, Ducasse L, Castet F. On the interface dipole at the pentacene-fullerene heterojunction: a theoretical study. *J Phys Chem C*, 2010, 114: 3215–3224
67 Cantrell RA, James C, Clancy P. Computationally derived rules for persistence of C_{60} nanowires on recumbent pentacene bilayers. *Langmuir*, 2011, 27: 9944–9954
68 Minami T, Nakano M, Castet Fdr. Nonempirically tuned long-range corrected density functional theory study on local and charge-transfer excitation energies in a pentacene/C_{60} model complex. *J Phys Chem Lett*, 2011, 2: 1725–1730
69 Muccioli L, D'Avino G, Zannoni C. Simulation of vapor-phase deposition and growth of a pentacene thin film on C60 (001). *Adv Mater*, 2011, 23: 4532–4536
70 Lii JH, Allinger NL. Molecular mechanics. The MM3 force field for hydrocarbons. 3. The van der Waals' potentials and crystal data for aliphatic and aromatic hydrocarbons. *J Am Chem Soc*, 1989, 111: 8576–8582
71 Fu YT, Risko C, Bredas JL. Intermixing at the pentacene-fullerene bilayer interface: a molecular dynamics study. *Adv Mater*, 2013, 25: 878–882
72 Drummy LF, Miska PK, Alberts D, Lee N, Martin DC. Imaging of crystal morphology and molecular simulations of surface energies in pentacene thin films. *J Phys Chem B*, 2006, 110: 6066–6071
73 Cheng HL, Lin JW. Controlling polymorphic transformations of pentacene crystal through solvent treatments: an experimental and theoretical study. *Cryst Growth Des*, 2010, 10: 4501–4508
74 Desai TV, Woll AR, Engstrom JR. Thin film growth of pentacene on polymeric dielectrics: unexpected changes in the evolution of surface morphology with substrate. *J Phys Chem C*, 2012, 116: 12541–12552
75 Ruiz R, Choudhary D, Nickel B, Toccoli T, Chang KC, Mayer AC, Clancy P, Blakely JM, Headrick RL, Iannotta S, Malliaras GG. Pentacene thin film growth. *Chem Mater*, 2004, 16: 4497–4508
76 Northrup JE, Tiago ML, Louie SG. Surface energetics and growth of pentacene. *Phys Rev B*, 2002, 66: 121404
77 Drummy LF, Martin DC. Thickness-driven orthorhombic to triclinic phase transformation in pentacene thin films. *Adv Mater*, 2005, 17: 903–907
78 Feng M, Lee J, Zhao J, Yates JT Jr, Petek H. Nanoscale templating of close-packed C_{60} nanowires. *J Am Chem Soc*, 2007, 129: 12394–12395
79 Guo YJ, Karasawa N, Goddard WA. Prediction of fullerene packing in C_{60} and C_{70} crystals. *Nature*, 1991, 351: 464–467
80 Ma X, Wigington B, Bouchard D. Fullerene C60: surface energy and interfacial interactions in aqueous systems. *Langmuir*, 2010, 26: 11886–11893
81 Neel N, Kroger J, Berndt R. Highly periodic fullerene nanomesh. *Adv Mater*, 2006, 18: 174–177
82 Pawlak R, Kawai S, Fremy S, Glatzel T, Meyer E. Atomic-scale mechanical properties of orientated C_{60} molecules revealed by noncontact atomic force microscopy. *Acs Nano*, 2011, 5: 6349–6354
83 Xiao WD, Ruffieux P, Ait-Mansour K, Groning O, Palotas K, Hofer WA, Groning P, Fasel R. Formation of a regular fullerene nanochain lattice. *J Phys Chem B*, 2006, 110: 21394–21398
84 Zhang HL, Chen W, Huang H, Chen L, Wee AT. Preferential trapping of C60 in nanomesh voids. *J Am Chem Soc*, 2008, 130: 2720–2721
85 Zimmerman JD, Xiao X, Renshaw CK, Wang S, Diev VV, Thompson ME, Forrest SR. Independent control of bulk and interfacial morphologies of small molecular weight organic heterojunction solar cells. *Nano Lett*, 2012, 12: 4366–4371
86 McMahon DP, Cheung DL, Troisi A. Why holes and electrons separate so well in polymer/fullerene photovoltaic cells. *J Phys Chem Lett*, 2011, 2: 2737–2741
87 Körzdörfer T, Sears JS, Sutton C, Bredas JL. Long-range corrected hybrid functionals for pi-conjugated systems: dependence of the range-separation parameter on conjugation length. *J Chem Phys*, 2011, 135: 204107
88 Pandey L, Doiron C, Sears JS, Bredas JL. Lowest excited states and optical absorption spectra of donor-acceptor copolymers for organic photovoltaics: a new picture emerging from tuned long-range corrected density functionals. *Phys Chem Chem Phys*, 2012, 14: 14243–14248
89 Körzdörfer T, Parrish RM, Sears JS, Sherrill CD, Bredas JL. On the relationship between bond-length alternation and many-electron self-interaction error. *J Chem Phys*, 2012, 137: 124305
90 Körzdörfer T, Parrish RM, Marom N, Sears JS, Sherrill CD, Brédas JL. Assessment of the performance of tuned range-separated hybrid density functionals in predicting accurate quasiparticle spectra. *Phys Rev B*, 2012, 86: 205110

91 Grimm B, Risko C, Azoulay JD, Bredas JL, Bazan GC. Structural dependence of the optical properties of narrow bandgap semiconductors with orthogonal donor-acceptor geometries. *Chem Sci*, 2013, 4: 1807–1819
92 Zhang CR, Coropceanu V, Sears JS, Bredas JL. Vibronic coupling in the ground state of oligoacene cations: the performance of range-separated hybrid density functionals. *J Phys Chem C*, 2014, 118: 154–158
93 Ryno SM, Lee SR, Sears JS, Risko C, Brédas JL. Electronic polarization effects upon charge injection in oligoacene molecular crystals: description via a polarizable force field. *J Phys Chem C*, 2013, 117: 13853–13860
94 Ryno SM, Risko C, Bredas JL. Impact of molecular packing on electronic polarization in organic crystals: the case of pentacene vs tips-pentacene. *J Am Chem Soc*, 2014, 136: 6421–6427
95 Burke TM, McGehee MD. How high local charge carrier mobility and an energy cascade in a three-phase bulk heterojunction enable > 90% quantum efficiency. *Adv Mater*, 2014, 26: 1923–1928